Dielectric relaxation and AC conductivity mechanism of eco-friendly Fe_2O_3 hexagonal nanomorphotype

T. PAULOSE, K. E. ABRAHAM*
St. Berchmans College, Changanacherry, Kerala, 686 101, India

We report dielectric and electron transport properties of hydrothermally synthesized ecofriendly Fe_2O_3 hexagonal nanomorphotype. The space charge polarization and orientational polarizations are the main mechanisms behind the dielectric property of Fe_2O_3 nanostructure. The frequency and temperature dependent impedance analysis was carried out in the frequency range 100Hz-1MHz. By theoretical fitting methods, the dielectric relaxation formalism has been identified as the Cole-Cole like relaxation. The AC conductivity in the nanomorphotype obeys the universal power law and also the frequency exponent parameter "s" decreases with increase in temperature. Correlating the nature of "s" with various theoretical models and observing that the conduction mechanism is mostly due to the thermally activated charge carriers, both overlapped polaron hopping transport (OLPT) and correlated barrier hopping (CBH) theoretical models are found to be valid in the present case. The dielectric study of Fe_2O_3 hexagonal nanomorphotype opens up the way for developing charge storage devices with least environmental hazard.

(Received March 21, 2016; accepted June 7, 2017)

Keywords: Fe_2O_3 hexagonal nanomorphotype, Dielectric properties, Impedance spectroscopy, AC conductivity

1. Introduction

The researchers in nanoregime have great interest to extract the dielectric behavior of semiconductor metal oxide nanomaterials. The semiconductor metal oxide nanomaterials show huge dielectric constant in nano range compared to its bulk microstructure [1-3]. The high dielectric constant materials are used in various technological applications like wireless communication systems, high energy storage devices, space missions, etc [4]. But still, the efficient dielectric as well as materials used in electronic industry has made huge negative environmental impact on earth surface/atmosphere. After the usage, scientific world are least concerned about the disposals of these materials. Meanwhile more research is being carried out to find better ecofriendly materials for electronic/industrial applications. Many more recent studies show Fe_2O_3 nanostructures are an ecofriendly material [5-7]. The present study is to put forward the ideas of dielectric and electron transport property of more ecofriendly Fe_2O_3 hexagonal nanomorphotype for electronic applications.

Recently, nanostructured Fe_2O_3 has received great attention due to its variety of applications in the field of energy, environmental studies, pigment for paint industry, and contrasting agent for medical diagnostics, magnetic resonance imaging and many other biomedical applications [8, 9]. In recent years, researchers have fabricated different morphotypes of iron oxide nanomaterials. For instance, Aaron M et al. reveal three iron oxide polymorphs, hematite, maghemite and magnetite grown on KBr substrates and its vibrational spectroscopic analysis [10]. Albert G. Nasibulin et al.and Huey-Wen Liou et al reported the Raman spectroscopic and hyperthermia therapy study of Fe_2O_3 nanowires respectively [11, 12]. Nitin Kaduba Chaudhari et al. and De Mont ferrand C et al. fabricated environment friendly hexagonal shaped Fe_2O_3 nanocrystals [13, 14]. However, there is lack of detailed reports from the dielectric properties of nanomaterials with hexagonal shapes especially in Fe_2O_3 nanostructures. N. N. Mallikarjuna and team reported the novel high dielectric constant nano composites of polyaniline dispersed with α-Fe_2O_3 nanoparticles and they suggested that conductivity and dielectric constant values are increased by increasing the amount of α-Fe_2O_3 in the matrix [15]. S. I. Srikrishna Ramya and C. K. Mahadevan conducted a work on the effect of calcination on the electrical properties and quantum confinement of Fe_2O_3 nanoparticles and reported that dielectric property is strongly dependent to quantum confinement effect [16]. S.K. Sahoo et.al studied the characterization of γ and α -Fe_2O_3 nano powders synthesized by emulsion precipitation-calcination route and also examined the rheological behavior of α -Fe_2O_3 [17]. S. M. Reda tested the electric and dielectric properties of Fe_2O_3/Silica nanocomposites and suggested that AC conductivity and dielectric loss of these composites increased gradually with increasing both annealing temperature and particle size [18]. S. S. Shinde and coworkers fabricated the hematite α -Fe_2O_3 thin films and examined its application to photoelectron chemical solar cells [19]. M. V. N. Ambika Prasad et.al studied the electrical and sensing properties of Polyaniline / Iron Oxide nanocomposites and reported that prepared nanocomposite has potential application in sensor devices [20].

Out of these facets, no literature is available for dielectric and electron transport properties of Fe_2O_3 nanomaterial in hexagonal morphology. In the present work, we investigated the dielectric relaxation and AC conductivity of Fe_2O_3 hexagonal shaped nanostructure synthesized by using the hydrothermal method. The conductivity relaxation time is determined from cole-cole model impedance spectroscopic analysis. The electrical studies show that dielectric permittivity of Fe_2O_3 hexagonal shaped nanostructure increases as compared with bulk. Both immense dielectric response and ecofriendly nature of Fe_2O_3 hexagonal nanomorphotype open up the ways for electronic industry to develop least environmental hazardous electronic devices.

2. Materials and method

We had reported an effective method for the synthesis of hexagonal shape Fe_2O_3 nanostructure through hydrothermal method in our recent AIP-Journal of Applied Physics paper [21]. $Fe(NO_3)_3.9H_2O$ and $(CH_2)_6N_4$ from Merck India Ltd (99.99%) are the reactants used. The crystal structure of the samples has been analyzed using X-ray diffraction analysis (Bruker AXS D8 Advance) with X-ray source Cu, of Wavelength 1.5406 Å. The molecular structure and chemical bonding of the prepared sample have been substantiated by recording the infrared (IR) spectra (Nicolet Nexus-670 FTIR spectrometer). Sample morphology was studied using high resolution transmission electron microscope (JEM-2100, 200 kV, Jeol). The fundamental optical band gap has been investigated through optical reflection/absorption spectroscopy (T90+ UV/Vis spectrometer). Photoluminescence (PL) analysis was performed with spectrofluorometer (Shimadzu, RF-5301 PC) using 150W Xenon lamp as excitation source. All these results have already been published [21]. For electrical analysis, the prepared powder sample was pelletized at a pressure of 2.5 tons for 5 minutes using a KBr hydraulic press. Silver paste was coated on both sides of the pellet for creating better contact between the pellet and the electrodes. The pellet had its diameter 13 mm and thickness 1.3 mm. The pellet was put in a furnace of varying temperature. The dielectric spectra, impedance spectra and AC conductivity measurements were carried out using a HIOKI 3532-50 LCR meter.

3. Results and discussion

3.1. Dielectric measurements

The variation of dielectric constant (ε') and loss tangent ($\tan\delta$) as a function of frequency for selected temperatures is presented in Fig. 1. It portrays that the dielectric constant for all the temperatures have high value at low frequencies as compared to that of the bulk Fe_2O_3. The nature of variation of dielectric constant and dielectric loss values are almost same, i.e. they rapidly decrease at first and reach to the constant values at all temperatures by the increment of frequency. This behavior can be explained with different polarization mechanisms involved in the semiconductor materials.

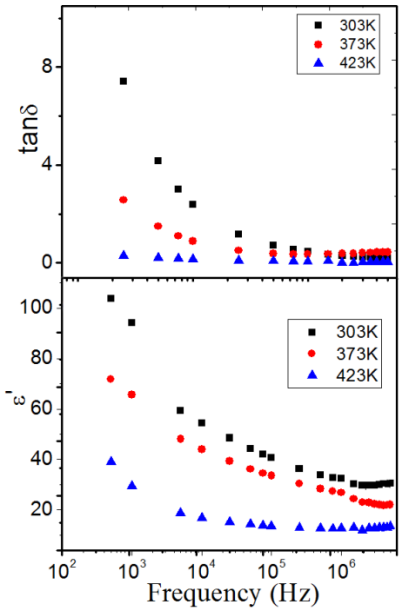

Fig. 1. Variation of dielectric constant and loss tangent with frequency at selected temperatures

A dielectric material is made up of large number of atoms/molecules that possess different types of electric polarizations such as electronic, atomic/ionic, dipolar, orientational or hopping and space charge polarizations. The space charge, orientational and atomic /ionic polarizations are significant only in low frequency AC field, whereas electronic polarizations are more significant in high frequency AC field. The lager period in low frequency provides sufficient time for the orientational or hopping, atomic/ionic and space charge polarizations and depolarization or relaxation which is quite large and varies in a wide range depending upon the dielectric system. Such polarizations are sometimes referred to as relaxation processes because they involve relaxation time. The relaxation phenomena are defined as the restoring action to bring the excited system back to its original equilibrium state. The response time for electronic polarization is short and can be assumed to be practically constant for all frequencies. Out of these facets, the large values of ε' and $\tan\delta$ at frequency region of around 10^4 Hz is mostly due to the involvement of space charge and orientational polarizations. Nanocrystalline semiconductor materials have large number of surface defects, interstitial sites, ionic vacancies, etc formed due to high surface to volume ratio and quantum confinement effect [22]. These imperfections generate positive and negative space charge distributions at the interstitial sites or defect levels. When an AC electrical field is applied, these space charges are moved and trapped in the defect/interface level resulting in the formation of dipole moment called space charge polarization. Meanwhile in Fe_2O_3 hexagonal shaped nanomaterials, enormous numbers of oxygen vacancies

(O^{2-}) and interstitial iron (Fe^{3+}) ions are created within the forbidden energy gap. These dipoles alter the orientation as per the direction of AC applied field, which is called as orientational polarization. Both space charge and orientational polarization mechanisms are contributing to the high dielectric constant value at lower frequencies.

Fig. 2 elucidates the temperature dependency of ε' and $\tan\delta$ of Fe_2O_3 hexagonal nanomorphotype at selected frequencies. Both ε' and $\tan\delta$ increase with temperature. As the temperature increases the oxygen vacancies are created and space charge polarization is enhanced. According to the ohmic conduction, as the temperature increases the electrical conductivity of semiconductor material also increases due to the mobility of thermally activated electrons. As a result, the dielectric polarization is dominated and results in high value of ε' at higher temperature. Meanwhile the huge value of $\tan\delta$ at higher temperature region is due to the conversion of large amount of energy to heat formed by the thermal agitation of electron.

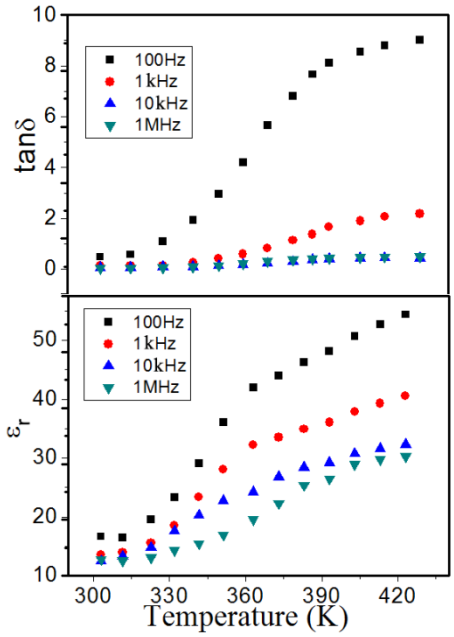

Fig. 2. Variation of dielectric constant and loss tangent with temperature at selected frequencies

3.2. Impedance spectroscopy

The detailed understanding of dielectric behavior, polarization effect and electrical transport property is obtained by analyzing the impedance spectroscopy [23-25]. The complex impedance analysis is used to determine the grain, grain boundary and electrode contribution in the case of dielectric materials. The impedance spectroscopy shows the frequency dependence of real part of impedance (Z^{I}) and imaginary part of impedance (Z^{II}). Polarizations can be grouped into two: the polarization in resonance region and the polarization in relaxation region. The polarization associated with vibration of electrons or vibration of atoms/ions belongs to resonance region because resonance will occur when the frequency of excited field is close to the natural frequency of oscillation system. Polarizations by orientational polarization or hopping and space charge polarization belong to the relaxation region. The relaxation phenomena occur only when the time required for the charge carriers to overcome the inertia is available. The Cole-Cole (the variation of Z^{I} *Vs* Z^{II} with frequency) plots of Fe_2O_3 hexagonal nanomorphotype at 303, 373 and 423 K are elucidated in Fig. 3a. It is clear that at all temperatures considered Z^{I} *Vs* Z^{II} curve appears like a 'depressed single semicircle', the diameter of which represents the resistance of the medium. In the present case the order of the resistance is in $K\Omega$ range. This behavior strongly supports the response of grain resistance in nanostructures [26]. Generally, Cole-Cole plots of semiconductor nanomaterials consist of one or more 'depressed semicircles' depending upon the temperature range [27, 28]. The diameters of these arcs represent electrical resistance due to grain, grain boundary, electrode etc. In the present case, a 'depressed single semicircle' type arc is obtained which is due to the study below 473 K. The semicircle diameter gives the electrical resistance (R) of the sample at a particular temperature and relaxation frequency $\omega = 1/RC$, where C is the capacitance. For scrutinizing the impedance spectra, the experimental data are modified through an equivalent circuit which consists of a resistor and a capacitor. The proposed equivalent circuit used for simulating the experimental data in the present work is the combination of a series resistor R_s with a parallel R_g and C_g element as shown in the Fig. 3a (inset) [29]. Here R_s represents the contact resistance of sample with the electrodes, R_g and C_g are resistance and capacitance values in the grain interior of Fe_2O_3 nanostructure. The Cole-Cole equation for impedance spectroscopic analysis is given by [30-33].

$$Z^{*} = Z^{'} - iZ^{''} \tag{1}$$

Where,

$$Z^{'} = \frac{Rg}{1+(\omega RgCg)^2} + \frac{Rgb}{1+(\omega RgbCgb)^2} \tag{2}$$

and,

$$Z^{''} = Rg\left[\frac{\omega RgCg}{1+(\omega RgCg)^2}\right] + Rgb\left[\frac{\omega RgbCgb}{1+(\omega RgbCgb)^2}\right] \tag{3}$$

The impedance spectrum (Fig. 3(a)) analyzed by Eq. 2 shows that the response peak from grain boundary are too weak. Therefore, by ignoring the second term in Eqn. 2, the Cole-Cole modification of Debye equation for impedance spectroscopic analysis for the present polycrystalline sample can be written as [34]

$$Z^{*} = \frac{Rg}{1+(\omega RgCg)^{\alpha}} \tag{4}$$

and the parameter α, $0<\alpha<1$ is used to find out the deviation from the ideal Debye response. Therefore a single parallel R_g and C_g combination is found to be the best fit with the experimental data for Fe_2O_3 hexagonal nanomorphotype. The value of R_g is obtained from the intercept of impedance semicircle on X-axis. The mean relaxation time is obtained from the relation $\tau_g = RgCg$, which is the inverse of the most intense frequency ω_g of the impedance spectrum. The grain parameters of Fe_2O_3 hexagonal nanomorphotype obtained by fitting the experimental data to Eq. 4 are reported in Table 1.

Table 1. The grain parameters of Fe_2O_3 hexagonal nanomorphotype by numerical fit to the experimental data points using Eq. 4

Temperature (K)	$R_g(\Omega)$	$C_g(F)$	$\tau_g(S)$	α
303	86430	3.93E-11	3.40E-06	0.52
373	60788	3.94E-11	2.40E-06	0.65
423	16429	4.06E-11	6.66E-07	0.69

The resistances obtained at all temperatures considered are in the order of $K\Omega$ range which indicates the polycrystalline nature grain response of the sample. Therefore, impedance spectroscopic measurement of Fe_2O_3 nanostructure gives grain resistance and corresponding capacitance in 100Hz-1MHz frequency region. It is noticed that the grain interior resistance and relaxation time are decreased with corresponding increment of temperatures. The obtained α values for different temperatures are evident for Cole-Cole relaxation of Fe_2O_3 hexagonal nanomorphotype or the departure from Debye behavior, which is further supported by Fig. 3b. In Fig. 3b, the relaxation frequency is shifted with respect to increasing in temperature which proves the Cole-Cole relaxation mechanism. The activation energy of Fe_2O_3 hexagonal nanomorphotype was calculated by fitting the data through Arrhenius equation [35, 36].

$$\sigma_g = \sigma_0 e^{\left(-Ea/k_BT\right)} \tag{5}$$

Here, E_a is the activation energy for conduction through grains. The activation energy is the energy required for a material to once start the conduction process which mainly depends on the temperature and size of the nanomaterial. The activation energy obtained for Fe_2O_3 hexagonal nanomorphotype is 0.0664 eV (Fig. 4).

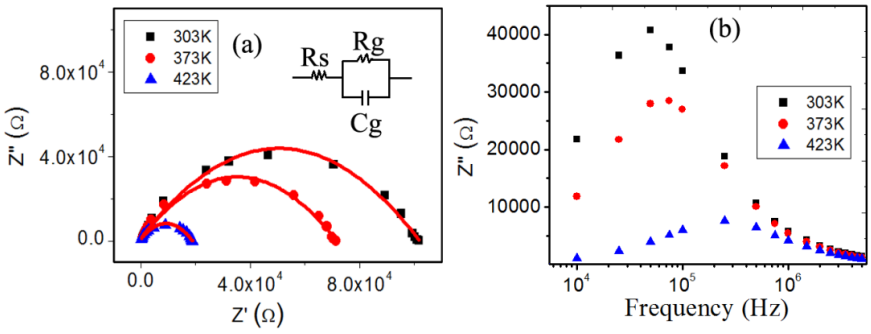

Fig. 3. (a) Complex impedance plot (Z^{II} Vs Z^{I}) at different temperatures, (b) Z^{II} Vs frequency curve

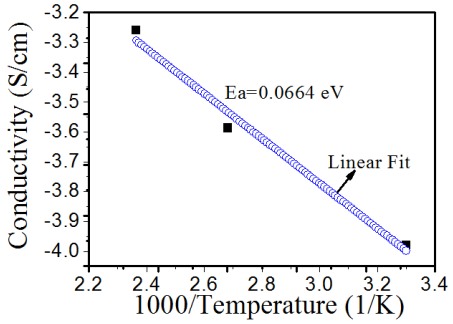

Fig. 4. Activation energy is obtained by numerical fit to the data points using Eq. 5

3.3. AC Conductivity measurements

The variation of electrical conductivity σ_{ac} with frequencies and temperatures at selected temperatures and frequencies are shown in Fig. 5 (a, b) respectively. The σ_{ac} is calculated by using the relation [37, 38].

$$\sigma_{ac} = \varepsilon' \varepsilon_0 \omega \tan\delta \tag{6}$$

In Fig. 5, the AC conductivity increases with the increase in both frequency and temperature. It is clear that from Fig. 5(a), ~~that~~ the AC conductivity has a constant nature up to the frequency range around 10^6 Hz, beyond

which there is a sharp increase in conductivity. Whereas, when temperature increases from 303 to 423K, the conductivity also increases. The increase in conductivity with temperature is the characteristic behavior of a thermally stimulated process and is attributed to the increase of the charge carrier's energy with the rise in temperature.

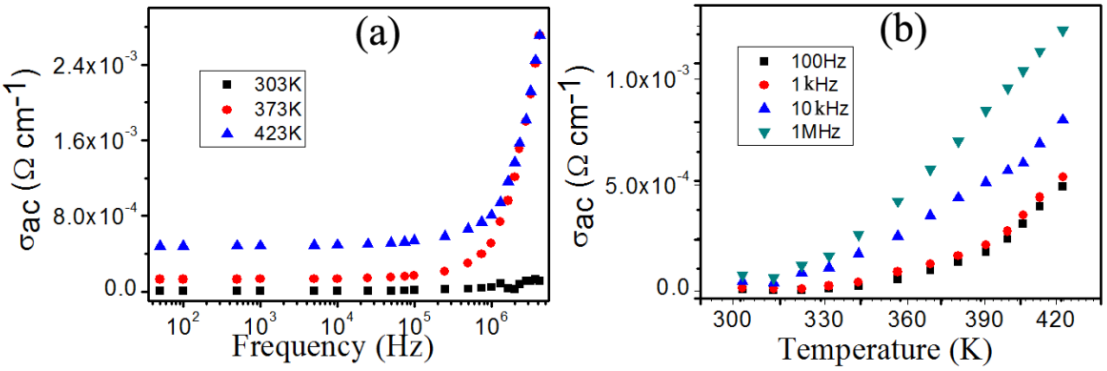

Fig. 5. Variation of σ_{ac} (a) with frequency at selected temperatures, (b) with temperature at selected frequencies

The conductivity mechanism in Fe_2O_3 hexagonal nanostructure obeys the universal power law in the form [39, 40]

$$\sigma_{ac} = A\omega^s \tag{7}$$

where A is a frequency independent constant. The exponent s is a frequency dependent parameter, its value lies in the range 0 < s < 1. The value of s defines the type of charge transport in the material. For detailed understanding of the type of charge transport behavior occurring in the nanostructure, s is estimated by fitting the experimental data using Eq. 7. The s values are plotted against temperatures are depicted in Fig. 6.

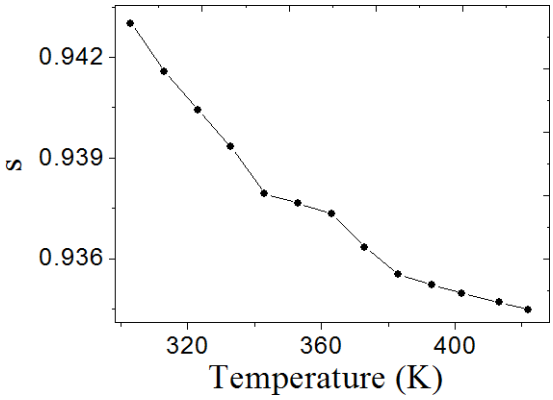

Fig. 6. Variations of s value with temperature

To study the nature of conduction in Fe_2O_3 hexagonal nanomorphotype on the basis of frequency exponent parameter s we consider different electron transport models such as quantum mechanical tunneling (QMT), overlapped polaron hopping transport (OLPT) and correlated barrier hopping (CBH). In QMT electrons travels from one lattice site to another, if the lattice sites are keeping a well ordered vibrational phase connection between them. In the CBH model thermally activated electrons shift from one lattice site to another even if there is no phase connection between them. QMT is a coherent process whereas CBH is an incoherent one.

In QMT the frequency exponent s is calculated by the equation [41, 42]

$$s = 1 - 4/\ln(\omega\tau_0) \tag{8}$$

where τ_0 is the relaxation time. The above equation shows the temperature independent but frequency dependent relation for the exponent s.

In overlapped polaron hopping transport (OLPT) model, the exponent s is given by [43-45]

$$s = 1 - \frac{8\alpha R + (6\beta W_{HO} r_p / R)}{\left(2\alpha R + (\beta W_{HO} r_p / R)\right)^2} \tag{9}$$

Here r_p is the polaron radius, R is intersite separation, $W_{HO} = e^2/4\varepsilon_p r_p$, α is spatial extent of polaron and $\beta = 1/K_B T$. As per Eq. 9, s should be temperature dependent. As the temperature increases the exponent decreases from unity.

Whereas, in correlated barrier hopping (CBH) model [46, 47]

$$s = 1 - \frac{6k_B T}{W_M + k_B T \ln(\omega\tau_0)} \tag{10}$$

In CBH model also, the exponent s shows temperature dependent nature. In this model s has maximum value in the low temperature region. In Fe_2O_3 hexagonal nanomorphotype, as seen in Fig. 6, the exponent s decreases from unity with corresponding increment in temperature. This indicates that conductivity is mostly by the hopping of charge carriers through the localized site.

At lower temperature the conductivity is mainly by hopping, while at higher temperature free band to band conduction is more prominent. Therefore it is robustly concluded that both CBH and OLPT transport model mechanisms are valid in Fe_2O_3 hexagonal nanostructure.

4. Conclusion

The dielectric and electron transport properties of hydrothermally synthesized ecofriendly Fe_2O_3 hexagonal nanomorphotype is carried out. The dielectric constant value is higher as compared with bulk Fe_2O_3. The main mechanism behind the dielectric behavior is from space charge polarization and orientational polarization. The impedance data is fitted with theoretical model and detected as the Cole-Cole like relaxation formalism. From AC conductivity analysis, the frequency exponent parameter "s" is calculated by theoretical fitting. It is found that the parameter "s" decreases with increase in temperature. Correlating the nature of "s" with various theoretical models and observing that the conduction mechanism is mostly due to the thermally activated charge carriers, it can be concluded that both overlapped polaron hopping transport (OLPT) and correlated barrier hopping (CBH) theoretical models are valid in the present case.

References

[1] Zhi-Min Liao, Kai-Jian Liu, Jing-Min Zhang, Jun Xu, Da-Peng Yu, J. Phys. Lett. A **367**(3), 207 (2007).
[2] Zhimin Dang et al., J. Mat. Res. Bull. **38**, 499 (2003).
[3] S. Ramasamy, B. Purniah, PINSA **67**, 85 (2001).
[4] B. Renner et al., J. Appl. Phys. **96**, 4400 (2004).
[5] Saptarshi Chatterjee, Arghya Bandyopadhyay, Keka Sarkar, J. Nanobiotechnology **9**, 34 (2011).
[6] Azam et al, Int. J. Nanomedicine **7**, 6003 (2012).
[7] Sudhanshu Shekhar Behera, Jayanta Kumar Patra, Krishna Pramanik, Niladri Panda, Hrudayanath Thatoi, World J. Nano Sci. and Eng. **2,** 196 (2012).
[8] M. F. Al-Kuhaili, M. Saleem, S. M. A. Durrani, J. Alloys and Compounds **521,** 178 (2012).
[9] Ming Ma, Yu Zhang, Zhirui Guo, Ning Gu, Nanoscale Res. Lett. **8,** 16 (2013).
[10] Aaron M. Jubb, Heather C. Allen, Appl. Materials and interfaces **2**, 10 (2010).
[11] Albert G. Nasibulin, Simas Rackauskas, Hua Jiang, Ying Tian, Prasantha Reddy Mudimela, Sergey D. Shandakov, Larisa Nasibulina, Jani Sainio, Esko I. Kauppinen, Nano Res. **2**, 373 (2009).
[12] Huey-Wen Liou, Hong-Ming Lin, Yeu-Kuang Hwu, Wen-Chang Chen, Wei-Jen Liou, Li-Chung Lai, Wei-Syuan Lin, Wen-An Chiou, J. Biomaterials and Nanobiotechnology **1**, 50 (2010).
[13] Nitin Kaduba Chaudhari, Hyoung Chan Kim, Derac Son, Jong-Sung Yu, Cryst. Eng. Comm. **11**, 2264 (2009).
[14] C. De Montferrand, L. Hu, I. Milosevic, V. Russier, D. Bonnin, L. Motte, A. Brioude, Y. Lalatonne, Acta Biomater **9**, 6150 (2013).
[15] N. N. Mallikarjuna, S. K. Manohar, P. V. Kulkarni, A. Venkataraman, T. M. Aminabhavi, J. Appl. Polymer Sci. **97,** 1868 (2005).
[16] S. I. Srikrishna Ramya, C. K. Mahadevan, Int. J. Res. in Eng. and Tech. **3,** 570 (2014).
[17] S. K. Sahoo, K. Agarwal, A. K. Singh, B. G. Polke, K. C. Raha, Int. J. Eng. Sci. and Tech. **2**, 118 (2010).
[18] S. M. Reda, Int. J. Nano Sci. and Tech. **1**, 17 (2013).
[19] S. S. Shinde et.al, J. Semiconductors **32,** 013001 (2011).
[20] M. V. N.Ambika Prasad et al, Int. J. Eng, Res, and Applications **4,** 198 (2014).
[21] Paulose Thomas, P. Sreekanth, K. E. Abraham, J. Appl. Phys. **117**, 053103 (2015).
[22] Paulose Thomas, K. E. Abraham, J. lum. **158**, 422 (2015).
[23] Syed Mahboob, G. Prasad, G. S. Kumar, Bull. Mater. Sci, **29,** 347 (2006).
[24] Md. T. Rahman, C. V. Ramana, J. Appl. Phys. **116,** 164108 (2014).
[25] Yukta P. Timalsina et.al, J. Appl. Phys. **110,** 014901 (2011).
[26] M. A. L. Nobre, S. Lanfredi, J. Appl. Phys. **93,** 5576 (2003).
[27] Jiandong Fan et al, J. Phys. D: Appl. Phys. **45,** 415301 (2012).
[28] Baochang Cheng et al, J. Mater. Chem. **21,** 1907 (2011).
[29] D. C Sinclair, A. R West, J. Appl. Phys. **66,** 3850 (1989).
[30] Kenneth S. Cole, Robert H. Cole, J. Chem. Phys. **9,** 341 (1941).
[31] Hsin-Ming Cheng, Wei-Hao Chiu, Chia-Hua Lee, Song-Yeu Tsai, Wen-Feng Hsieh, J. Phys. Chem. C **112,** 16359 (2008).
[32] Bikramkeshari Das, Tanushree Das, Kajal Parashar, S. K. S. Parashar, Appl. Sci. and Adv. Mat. Int. **1,** 16 (2014).
[33] Tanushree Das, Bikram keshari Das, Kajal Parashar, S. K. S. Parashar, Appl. Sci. and Adv. Mat. Int. **1,** 28 (2014).
[34] Jianjun Liu, Chun-Gang Duan, Wei-Guo Yin, W. N. Mei, R. W. Smith, J. R. Hardy, Phys. Rev. B, **70,** 144106 (2004).
[35] N. Kılınç, L. Arda, S. Öztürk, Z. Z. Öztürk, Cryst. Res. Technol. **45**, 529 (2010).
[36] Asma Tabib, Nasr Sdiri, Habib Elhouichet, Mokhtar Férid, J. Alloys and Compounds **622**, 687 (2015).
[37] E. Muhammad Abdul Jamal, D. Sakthi Kumar, M. R. Anantharaman, Bull. Mater. Sci. **34,** 251 (2011).
[38] Rintu Mary Sebastian, Sheena Xavier, E. M. Mohammed, Int. J. Eng. Sci. and Inno. Tech. **2,** 512 (2013).

[39] R. N. Bhowmik, N. Naresh, Int. J. Eng. Sci. and Tech. **2,** 40 (2010).
[40] H. Erdemi, H. Sözeri, M. S. Enel, A. Baykal, J. Nanopart. Res. **14,** 988 (2012).
[41] R. Ondo-Ndong et al, Microelectronics Journal **34,** 1087 (2003).
[42] M. Pollack, T. H Geballe, Phy. Rev. **121,** 1742 (1961).
[43] M. Pollak, T. H Geballe, Phy. Rev. **122,** 1742 (1961).
[44] G. E Pike, Phy. Rev. B. **6,** 1572 (1972).
[45] E. Veena Gopalan, K. A. Malini, S. Saravanan, D. Sakthi Kumar, Yasuhiko Yoshida, M. R. Anantharaman, J. Phys. D: Appl. Phys. **41**, 185005 (2008).
[46] Safenaz M. Reda, Sheikha M. Al-Ghannam, Advances in Materials Physics and Chemistry **2**, 75 (2012).
[47] Shaker Ebrahim, Abdel-Hady Kashyout, Moataz Soliman, Curr. App. Phy. **9**, 448 (2009).

*Corresponding author: abrahamke@gmail.com